



Title	Comparative study of GeO <sub>2</sub> /Ge and SiO <sub>2</sub> /Si structures on anomalous charging of oxide films upon water adsorption revealed by ambient-pressure X-ray photoelectron spectroscopy
Author(s)	Mori, Daichi; Oka, Hiroshi; Hosoi, Takuji et al.
Citation	Journal of Applied Physics. 2016, 120(9), p. 095306-1-095306-10
Version Type	VoR
URL	<a href="https://hdl.handle.net/11094/83923">https://hdl.handle.net/11094/83923</a>
rights	Copyright 2016 Author(s). This article may be downloaded for personal use only. Any other use requires prior permission of the author and AIP Publishing. This article appeared in Journal of Applied Physics, 120(9), 095306, 2016 and may be found at <a href="https://doi.org/10.1063/1.4962202">https://doi.org/10.1063/1.4962202</a> .
Note	

*The University of Osaka Institutional Knowledge Archive : OUKA*

<https://ir.library.osaka-u.ac.jp/>

The University of Osaka

# Comparative study of GeO<sub>2</sub>/Ge and SiO<sub>2</sub>/Si structures on anomalous charging of oxide films upon water adsorption revealed by ambient-pressure X-ray photoelectron spectroscopy

Daichi Mori,<sup>1</sup> Hiroshi Oka,<sup>2</sup> Takuji Hosoi,<sup>2</sup> Kentaro Kawai,<sup>1</sup> Mizuho Morita,<sup>1</sup> Ethan J. Crumlin,<sup>3</sup> Zhi Liu,<sup>3</sup> Heiji Watanabe,<sup>2</sup> and Kenta Arima<sup>1,a)</sup>

<sup>1</sup>Department of Precision Science and Technology, Graduate School of Engineering, Osaka University, 2-1, Yamada-oka, Suita, Osaka 565-0871, Japan

<sup>2</sup>Department of Material and Life Science, Graduate School of Engineering, Osaka University, 2-1, Yamada-oka, Suita, Osaka 565-0871, Japan

<sup>3</sup>Advanced Light Source, Lawrence Berkeley National Laboratory, Berkeley, California 94720, USA

(Received 21 May 2016; accepted 22 August 2016; published online 2 September 2016)

The energy difference between the oxide and bulk peaks in X-ray photoelectron spectroscopy (XPS) spectra was investigated for both GeO<sub>2</sub>/Ge and SiO<sub>2</sub>/Si structures with thickness-controlled water films. This was achieved by obtaining XPS spectra at various values of relative humidity (RH) of up to ~15%. The increase in the energy shift is more significant for thermal GeO<sub>2</sub> on Ge than for thermal SiO<sub>2</sub> on Si above ~10<sup>-4</sup>% RH, which is due to the larger amount of water molecules that infiltrate into the GeO<sub>2</sub> film to form hydroxyls. Analyzing the origins of this energy shift, we propose that the positive charging of a partially hydroxylated GeO<sub>2</sub> film, which is unrelated to X-ray irradiation, causes the larger energy shift for GeO<sub>2</sub>/Ge than for SiO<sub>2</sub>/Si. A possible microscopic mechanism of this intrinsic positive charging is the emission of electrons from adsorbed water species in the suboxide layer of the GeO<sub>2</sub> film to the Ge bulk, leaving immobile cations or positively charged states in the oxide. This may be related to the reported negative shift of flat band voltages in metal-oxide-semiconductor diodes with an air-exposed GeO<sub>2</sub> layer. *Published by AIP Publishing.*

[<http://dx.doi.org/10.1063/1.4962202>]

## I. INTRODUCTION

The miniaturization of silicon (Si) metal-oxide-semiconductor field-effect transistors (MOSFETs) has been pursued in the last few decades with the aim of achieving both high performance and low power consumption. However, it is becoming increasingly challenging to scale down MOSFETs because of a variety of physical problems such as the short channel effect, gate leakage current, and parasitic resistance/capacitance. Because these problems lead to increased power consumption and the degradation of device performances, it is important to introduce a channel material with higher mobility than Si, which is expected to lead to higher device performances without relying on a conventional scaling scheme.

Germanium (Ge) is regarded as a promising channel material for future MOSFETs because of its higher holes and electron mobilities than those of Si.<sup>1,2</sup> Another advantage of Ge is its process compatibility with Si-based MOS technologies. Because of these advantages, various attempts have recently been made to fabricate Ge-based MOS devices. Although Ge oxide (GeO<sub>2</sub>) is the most fundamental insulator in these devices, it decomposes at low temperatures<sup>3,4</sup> and is soluble in water,<sup>5</sup> unlike the more familiar Si oxide (SiO<sub>2</sub>). In spite of these physical instabilities of the bulk, the GeO<sub>2</sub>/Ge interface is still attractive because of its excellent electrical properties.<sup>6</sup> Researchers have developed a wide range

of gate stack structures with a GeO<sub>2</sub>/Ge interface. One approach is to use thermal or plasma techniques such as nitridation to passivate a GeO<sub>2</sub> surface by forming a GeON layer on top of GeO<sub>2</sub>.<sup>7</sup> Another approach is to cap the GeO<sub>2</sub> surface by the deposition of high-*k* dielectric layers.<sup>8,9</sup> Metal-oxide-doped GeO<sub>2</sub> such as yttrium-GeO<sub>2</sub> has attracted interest because of its stronger resistance to liquid water than pure GeO<sub>2</sub>.<sup>10,11</sup>

The above studies indicate that GeO<sub>2</sub> is a key material in Ge-based MOSFETs, and it is still necessary to grasp the relationship between the physical/chemical properties of GeO<sub>2</sub> and its dielectric properties. Among these properties, the effect of the microscopic interaction of water vapor on the quality of the GeO<sub>2</sub>/Ge structure is a serious concern that should be clarified. Several groups have so far investigated this issue. Hosoi *et al.*<sup>12</sup> and Oniki *et al.*<sup>13,14</sup> reported the electrical characteristics of metal/GeO<sub>2</sub>/Ge structures and revealed a negative shift of the flat-band voltage (*V*<sub>FB</sub>) as well as anomalous hysteresis and a minority carrier response upon exposure to air. Diverse physical analyses such as by thermal desorption spectroscopy, infrared spectroscopy, and secondary ion mass spectrometry revealed the origin to be infiltration of adsorbed water or organic molecules into the GeO<sub>2</sub> film.<sup>12-15</sup>

X-ray photoelectron spectroscopy (XPS) is a powerful tool for identifying various properties of oxide/semiconductor structures. Analysis of the chemical shift of oxidation states is especially important for determining the oxide thickness, suboxide structure, and band offset. However, as Zhang *et al.*

<sup>a)</sup>Author to whom correspondence should be addressed. Electronic mail: [arima@prec.eng.osaka-u.ac.jp](mailto:arima@prec.eng.osaka-u.ac.jp)

pointed out,<sup>16</sup> this fundamental issue is still controversial in the case of GeO<sub>2</sub> films on Ge. Recently, we conducted ambient-pressure XPS (AP-XPS) measurements on an annealed GeO<sub>2</sub> film on Ge in water vapor and demonstrated that the chemical shift of the GeO<sub>2</sub> peak (Ge<sup>4+</sup>) from the bulk 3d<sub>5/2</sub> increases with increasing relative humidity (RH) up to 1%.<sup>17</sup> In the present study, we obtained more AP-XPS spectra with synchrotron radiated light to investigate the chemical shift of GeO<sub>2</sub> on Ge in the presence of a thin water film in detail. By comparing the results with those for SiO<sub>2</sub>/Si, we unveil the impact of the adsorption of water molecules on the quality of thin GeO<sub>2</sub> films on Ge.

## II. EXPERIMENTAL DETAILS

### A. Sample preparation

In most experiments, we used p-type Ge(100) and Si(100) wafers with resistivities in the range of 0.1–0.5  $\Omega$  cm and 0.1–6.0  $\Omega$  cm, respectively. Another n-type Si(100) wafer whose resistivity was less than 1  $\Omega$  cm was also sometimes used. For the Ge samples, we formed sacrificial oxides by dry oxidation at 450 °C for 30 min in a conventional furnace and cleaned them by cyclic treatment using dilute HF (5%) and ultrapure water. Then, thin GeO<sub>2</sub> films were formed on the Ge substrate by dry oxidation at 550 °C. The Si samples were rinsed with ultrapure water, cleaned with a H<sub>2</sub>SO<sub>4</sub>/H<sub>2</sub>O<sub>2</sub> solution, etched with a dilute HF solution (1%), and rinsed with ultrapure water. They were oxidized at 1000 °C in a cold-wall-type reaction chamber<sup>18</sup> in O<sub>2</sub> ambient. The GeO<sub>2</sub>/Ge and SiO<sub>2</sub>/Si samples were stored immediately in a vacuum desiccator evacuated by a diaphragm pump and were transferred to an AP-XPS chamber. All the Ge and Si samples were annealed at 300 °C for 30 min in a vacuum prior to the exposure to water vapor. This thermal treatment is referred to as preannealing hereafter.

### B. AP-XPS experiments

AP-XPS measurements were performed at beamline 9.3.2 of the Advanced Light Source (ALS) of the Lawrence Berkeley National Laboratory. The X-ray flux was approximately  $5 \times 10^{10}$  photons/s.<sup>19</sup> A differentially pumped electrostatic lens system separated the AP-XPS chamber from a hemispherical photoelectron spectrometer, which enabled us to collect photoelectrons in gases at pressures of up to several Torr.<sup>19–21</sup> The energy resolution of the beamline is about  $E/\Delta E = 3000$ .<sup>19</sup> We used commercial water (Aristar Plus HPLC, low TOC grade) from The British Drug Houses (BDH) with a total organic carbon content of less than 20 ppb as the source of the water vapor. After the water was degassed in freeze-pump-thaw cycles, it was introduced into the XPS chamber under an ultrahigh vacuum (UHV) condition at a pressure of up to 1.0 Torr. In this article, we define UHV as pressures lower than  $6 \times 10^{-8}$  Torr. We also controlled the sample temperature using a chiller, with which the lowest temperature achieved was  $-9.6$  °C. These procedures enabled us to obtain AP-XPS spectra in the humidity range of 0%–15%. The bulks of the Ge and Si samples were grounded.

Unless otherwise stated, the X-ray conditions were as follows. The spectra of the Ge 3d, Si 2p, O 1s, and C 1s core levels were obtained at incident photon energies of 350, 420, 855, and 610 eV, respectively. Because photoelectrons from these levels have similar kinetic energies of approximately 320 eV, we ensured that the probing depth was similar when obtaining the photoelectron spectra. The X-ray flux at 350 eV was similar to that at 420 eV. Ge 3d and Si 2p spectra were also collected at a photon energy of 855 eV. We obtained each spectrum by averaging at least three spectra to improve the signal-to-noise ratio; this took longer than 150 s. The pass energy was set to 100 eV. The binding energy scales of spectra taken on GeO<sub>2</sub>/Ge and SiO<sub>2</sub>/Si samples were calibrated using the known values for elemental Ge 3d<sub>5/2</sub> (29.36 eV) and Si 2p<sub>3/2</sub> (99.4 eV), respectively.<sup>22–24</sup> We used the NIST database to obtain the inelastic mean free path (IMEP) of electrons in Ge, Si, GeO<sub>2</sub>, SiO<sub>2</sub>, H<sub>2</sub>O, and C.<sup>25</sup>

The oxide thicknesses of the thermal GeO<sub>2</sub> and SiO<sub>2</sub> films were in the ranges of 1.4–2.8 nm and 1.7–3.7 nm, respectively, which were estimated from the Ge 3d or Si 2p spectra using the formula proposed by Himpsel *et al.*<sup>26</sup> We found that this estimation has an error of  $\pm 0.20$  nm due to statistical dispersion. Assuming 0.3 nm per carbon layer, the amount of carbon contamination was estimated to be 0.1–0.5 and 0.05–0.3 monolayers for GeO<sub>2</sub> and SiO<sub>2</sub> surfaces after preannealing, respectively. The contamination level on GeO<sub>2</sub> tended to be higher than that on SiO<sub>2</sub>, probably because a GeO<sub>2</sub> film absorbs organic molecules unlike SiO<sub>2</sub>.<sup>15</sup>

An O 1s spectrum together with a Ge 3d spectrum and a Si 2p spectrum were used to estimate the water layer thickness under an equilibrium condition on GeO<sub>2</sub> and SiO<sub>2</sub> surfaces, respectively. In the presence of water vapor, the O 1s spectrum after Shirley background subtraction included contributions from oxygen in the oxide film, in the adsorbed water species, and in the gas phase. Some examples of O 1s spectra are shown in Fig. 1. After the peaks were separated by peak fitting, the water layer thickness on the oxide surfaces was estimated from the separated peak areas. This was achieved by assuming a simple structure composed of three layers (water/oxide/semiconductor bulk). Details of this estimation are described elsewhere.<sup>17,27</sup> We found that the estimation of a peak area has a deviation of 5%. This leads to an error of about  $\pm 10\%$  in the calculated water layer thicknesses. Noted that we cannot distinguish molecular water from surface hydroxyls because the energy difference between these two signals in O 1s spectra is too narrow for them to be separated.<sup>17,28</sup>

## III. RESULTS AND DISCUSSION

Figure 2 shows XPS spectra obtained in UHV, whose investigation was the direct motivation of this study. Figure 2(a) was obtained after a GeO<sub>2</sub>/Ge sample stored in a vacuum desiccator was exposed to ambient air and then introduced into an AP-XPS chamber. There are two main peaks: one is from the Ge bulk (Ge<sup>0+</sup>) and the other is a chemical shift component from GeO<sub>2</sub> (Ge<sup>4+</sup>). We analyzed the positions of the Ge 3d<sub>5/2</sub> core line signals for the two components and found that the GeO<sub>2</sub>(Ge<sup>4+</sup>) Ge 3d<sub>5/2</sub> component is

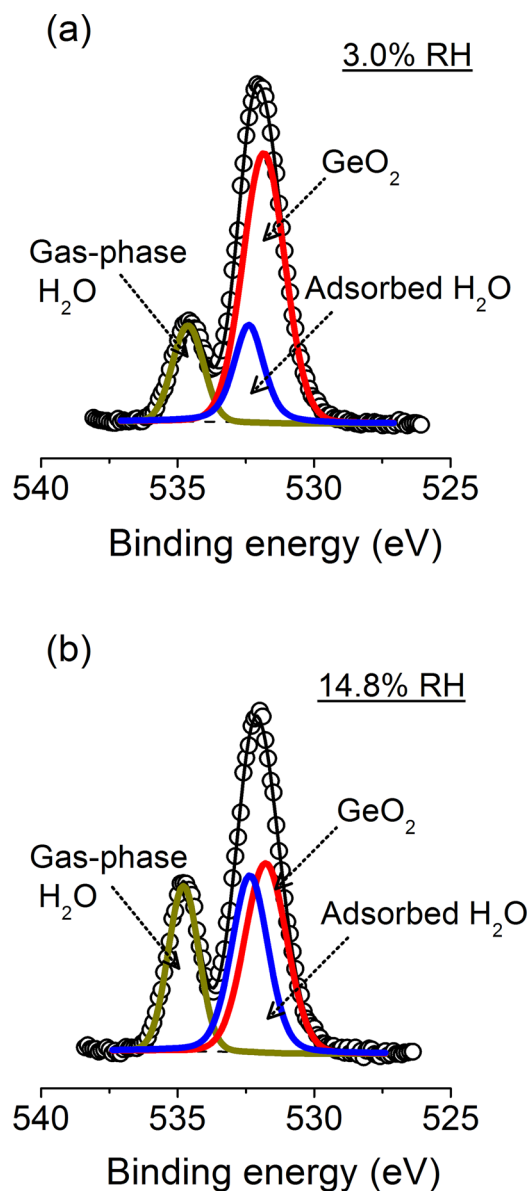


FIG. 1. Peak-fitted O 1s spectra on a  $\text{GeO}_2/\text{Ge}$  sample obtained at different values of RH. In each spectrum, the photoelectron intensity was normalized by the largest count. The area ratio of adsorbed water to the  $\text{GeO}_2$  bulk in (b) is higher than that in (a), which indicates the formation of a thicker water layer in (b). See Ref. 17 for the procedure used to determine the peak areas of  $\text{GeO}_2$  and adsorbed water in the O 1s spectra.

situated at 32.81 eV. This revealed that the energy difference between the two components is 3.45 eV in Fig. 2(a). We hereafter denote this energy difference, or the energy shift of the  $\text{GeO}_2$  peak ( $\text{Ge}^{4+}$ ) from the Ge bulk, as  $\Delta E_{\text{GeO}_2}$ . Figure 2(b) shows the spectrum after preannealing of the sample in Fig. 2(a). We did not expose the annealed sample to ambient air but kept it and obtained the spectrum in UHV. The binding energy of the  $\text{GeO}_2(\text{Ge}^{4+})$  Ge  $3d_{5/2}$  component in Fig. 2(b) was found to be 32.47 eV, indicating that  $\Delta E_{\text{GeO}_2}$  is 3.11 eV. This value is 0.34 eV smaller than that in Fig. 2(a), although the change in the oxide thickness (2.38 nm in Fig. 2(a) to 2.21 nm in Fig. 2(b)) is trivial. This decrease in the energy difference caused by the preannealing was not observed for  $\text{SiO}_2/\text{Si}$ . Namely, we conducted peak fitting of the measured spectra in Figs. 2(c) and 2(d) and analyzed the

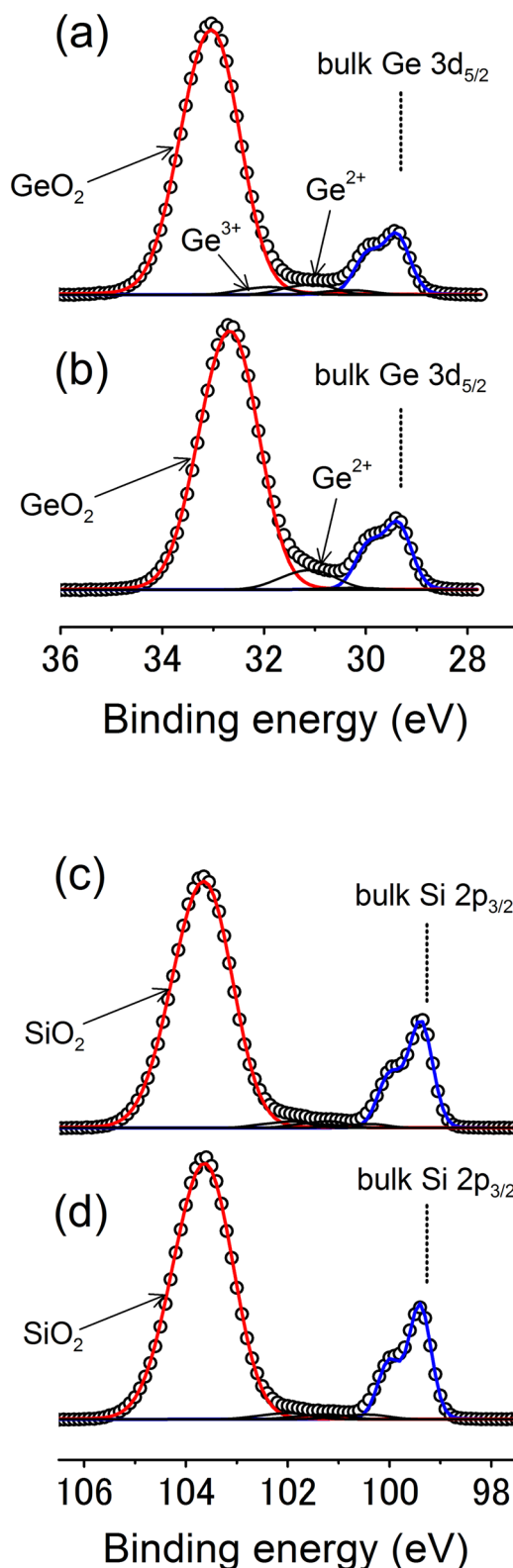


FIG. 2. Peak-fitted XPS spectra obtained in UHV. (a) Ge 3d spectrum of an air-exposed  $\text{GeO}_2/\text{Ge}$  sample. (b) Ge 3d spectrum after the sample in (a) was subsequently annealed at 300 °C for 30 min in a vacuum (preannealing). The shoulder peaks with binding energy close to 30 eV in (a) and (b) are both the Ge  $3d_{3/2}$  lines from the Ge bulk. (c) Si 2p spectrum of an air-exposed  $\text{SiO}_2/\text{Si}$  sample. (d) Si 2p spectrum after preannealing of the sample in (c). The shoulder peaks with binding energy close to 100 eV in (c) and (d) are both the Si  $2p_{1/2}$  lines from the Si bulk. The initial  $\text{GeO}_2$  and  $\text{SiO}_2$  thicknesses in (a) and (c) are 2.38 and 2.71 nm, respectively. The positions of the suboxide components ( $\text{Ge}^{1+}$ ,  $\text{Ge}^{2+}$ , and  $\text{Ge}^{3+}$ ) for the  $\text{GeO}_2/\text{Ge}$  sample are assigned from the literature,<sup>29</sup> whereas those for  $\text{SiO}_2/\text{Si}$  ( $\text{Si}^+$ ,  $\text{Si}^{2+}$ , and  $\text{Si}^{3+}$ ) were taken from another paper.<sup>26</sup>



positions of the Si 2p<sub>3/2</sub> signals for both the oxide (Si<sup>4+</sup>) and the substrate components. The SiO<sub>2</sub> (Si<sup>4+</sup>) Si 2p<sub>3/2</sub> components are situated at 103.51 and 103.48 eV in Figs. 2(c) and 2(d), respectively. Thus, we found that  $\Delta E_{\text{SiO}_2}$  changes from 4.11 eV in Fig. 2(c) to 4.08 eV in Fig. 2(d), where  $\Delta E_{\text{SiO}_2}$  represents the energy shift of the SiO<sub>2</sub> peak (Si<sup>4+</sup>) from the Si bulk. The SiO<sub>2</sub> thicknesses in Figs. 2(c) and 2(d) were 2.71 and 2.67 nm, respectively. The thermal desorption spectra of molecules desorbed from the thermally grown GeO<sub>2</sub> and SiO<sub>2</sub> films indicated that GeO<sub>2</sub> has an unusual characteristic in terms of its absorbability of water molecules in air.<sup>14,15</sup> This strongly implies that the absorbance of moisture is the origin of the change in  $\Delta E_{\text{GeO}_2}$  upon air exposure as shown in Figs. 2(a) and 2(b). It should be noted that the positions of the oxide and bulk peaks used to obtain  $\Delta E_{\text{GeO}_2}$  and  $\Delta E_{\text{SiO}_2}$  are influenced by the peak-fitting conditions such as the peak positions of the suboxides and the background subtraction. This results in errors in the calculated  $\Delta E_{\text{GeO}_2}$  and  $\Delta E_{\text{SiO}_2}$ . Unless otherwise stated, both  $\Delta E_{\text{GeO}_2}$  and  $\Delta E_{\text{SiO}_2}$  have an error of  $\pm 0.04$  eV.

Figure 3 shows water layer thicknesses as a function of relative humidity (RH). On the SiO<sub>2</sub> surface, the water coverage shows a rapid increase above 10<sup>-1</sup>% and reaches 0.3 nm at 10%. This corresponds to approximately one layer (assuming 0.3 nm per water layer), which agrees with previous measurements by other groups.<sup>28,30,31</sup> On the other hand, thicker water films are formed on a GeO<sub>2</sub> surface than on SiO<sub>2</sub> at RH higher than 10<sup>-4</sup>%, and one monolayer is achieved at a RH of approximately 1%. The thickness of the water layer rapidly increases above 1% RH, reaching 0.6–0.8 nm at 10% RH. Figure 3 demonstrates that a GeO<sub>2</sub> surface attracts a thicker water film than a SiO<sub>2</sub> surface in the RH range of 10<sup>-4</sup>% to 10%. As mentioned in Section II, we cannot separate the component of surface hydroxyls from that of molecular water in O 1s spectra because their binding

energies are too close. However, we speculate that the growth of the water layer on the GeO<sub>2</sub>/Ge samples in the RH range between 10<sup>-4</sup>% and around 1% in Fig. 3 mainly represents the hydroxylation of the GeO<sub>2</sub> film by the dissociative adsorption of water molecules. This is based on reports by other groups on the interaction of water vapor with the surfaces of various metal oxides including SiO<sub>2</sub>.<sup>28,32–35</sup> In these studies, it was argued that the hydroxylation precedes the growth of a molecular water film, and the former starts at an RH of much lower than 1%. After the saturation of hydroxyl formation at a RH of around 1%, the adsorption of molecular water begins as a result of the attractive interaction between H<sub>2</sub>O molecules and hydroxyls.<sup>36</sup> Considering the permeable nature of GeO<sub>2</sub>, it seems reasonable to conclude from Fig. 3 that hydroxylation not only of the GeO<sub>2</sub> surface but also in the GeO<sub>2</sub> film starts at  $\sim 10^{-4}$ % RH. The sudden increase in the thickness above  $\sim 1$ % RH in Fig. 3 indicates the formation of a molecular water film.

Next, we investigate the variation of both  $\Delta E_{\text{GeO}_2}$  and  $\Delta E_{\text{SiO}_2}$  with the thickness of the adsorbed water layer. This was achieved by obtaining the Ge 3d and Si 2p spectra at controlled values of RH on GeO<sub>2</sub> and SiO<sub>2</sub> surfaces, respectively. As shown in Fig. 4(a),  $\Delta E_{\text{GeO}_2}$  and  $\Delta E_{\text{SiO}_2}$  increase with RH for all GeO<sub>2</sub>/Ge and SiO<sub>2</sub>/Si samples. Moreover, we found that thicker oxide films tend to generate larger energy differences at a fixed RH. For example,  $\Delta E_{\text{GeO}_2}$  at  $\sim 1$ % RH is 3.67 and 3.47 eV on 2.73- and 1.85-nm-thick GeO<sub>2</sub> films, and  $\Delta E_{\text{SiO}_2}$  is 4.44, 4.19, and 4.07 eV on 3.69-, 2.71-, and 1.76-nm-thick SiO<sub>2</sub> layers, respectively. These increases in  $\Delta E_{\text{GeO}_2}$  and  $\Delta E_{\text{SiO}_2}$  for thicker oxide films are known to occur in both the GeO<sub>2</sub>/Ge and SiO<sub>2</sub>/Si systems under a dry condition in UHV. In particular, for the latter system, its origin has been widely discussed on the basis of the final-state effect and charge trapping.<sup>37–41</sup>

We calculated the change in the energy difference  $\Delta E_{\text{GeO}_2}$  or  $\Delta E_{\text{SiO}_2}$  at an elevated RH from that at the lowest RH or in UHV for each sample, which is defined as  $\Delta E_{\text{change}}$  hereafter. Namely, for both the GeO<sub>2</sub>/Ge and SiO<sub>2</sub>/Si samples

$$\Delta E_{\text{change}} = \Delta E_{\text{elevated RH}} - \Delta E_{\text{UHV}}, \quad (1)$$

in which  $\Delta E_{\text{elevated RH}}$  and  $\Delta E_{\text{UHV}}$  are  $\Delta E_{\text{GeO}_2}$  (or  $\Delta E_{\text{SiO}_2}$ ) at a controlled RH in water vapor and that in UHV, respectively. Figure 4(b) shows  $\Delta E_{\text{change}}$  obtained from the energy difference data in Fig. 4(a). Similar to  $\Delta E_{\text{GeO}_2}$  or  $\Delta E_{\text{SiO}_2}$ , as stated in an earlier paragraph, each plot of  $\Delta E_{\text{change}}$  has an error of  $\pm 0.04$  eV. In Fig. 4(b),  $\Delta E_{\text{change}}$  overlaps for the GeO<sub>2</sub> and SiO<sub>2</sub> surfaces up to 10<sup>-4</sup>% RH. However,  $\Delta E_{\text{change}}$  for the GeO<sub>2</sub>/Ge samples increases more significantly than that for the SiO<sub>2</sub>/Si ones at RH higher than 10<sup>-4</sup>%. Also, the total increase in  $\Delta E_{\text{GeO}_2}$  is 2–3 times larger than that in  $\Delta E_{\text{SiO}_2}$  at 10% RH. As we pointed out for Fig. 3, 10<sup>-4</sup>% is the critical RH around which the water layer starts to grow more rapidly on GeO<sub>2</sub> than on SiO<sub>2</sub>. It seems reasonable to suppose that the more rapid increase in  $\Delta E_{\text{GeO}_2}$  for GeO<sub>2</sub> above this critical RH in Fig. 4(b) is induced by the thicker water films than those on SiO<sub>2</sub>.

Figure 5 shows the recovery properties of  $\Delta E_{\text{GeO}_2}$  and  $\Delta E_{\text{SiO}_2}$  when the water vapor in the AP-XPS chamber was

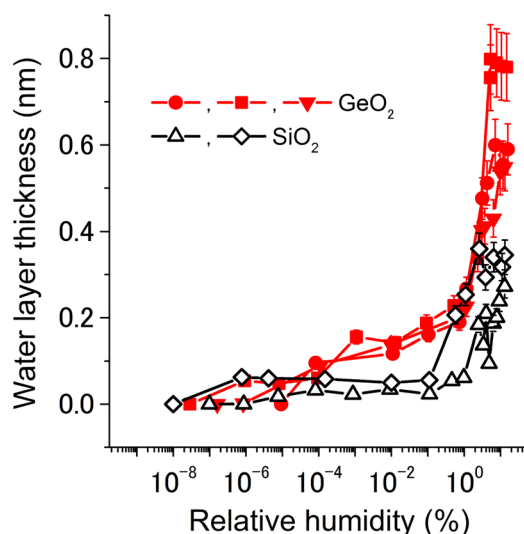


FIG. 3. Water layer thicknesses as a function of RH. Filled and open symbols represent data for GeO<sub>2</sub>/Ge and SiO<sub>2</sub>/Si, respectively. Symbols with different shapes indicate samples with different oxide thicknesses. Namely, the oxide thicknesses for the three GeO<sub>2</sub> samples were in the range between 1.8 nm and 2.8 nm, whereas those for the two SiO<sub>2</sub> samples were approximately 2.7 nm.

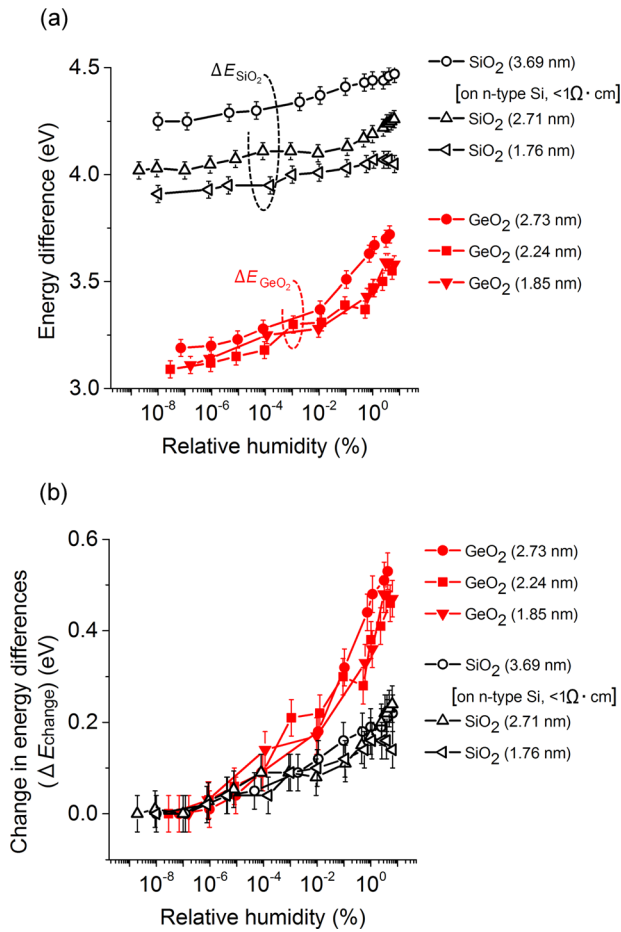


FIG. 4. (a)  $\Delta E_{\text{GeO}_2}$  (filled symbols) and  $\Delta E_{\text{SiO}_2}$  (open symbols) as a function of RH. Oxide thicknesses are indicated in parentheses in the legends. Most oxides were formed on p-type substrates except for the 3.69-nm-thick SiO<sub>2</sub> layer formed on an n-type substrate. (b) Changes in  $\Delta E_{\text{GeO}_2}$  or  $\Delta E_{\text{SiO}_2}$  at elevated RH from those taken in UHV, denoted as  $\Delta E_{\text{change}}$ , for each sample in (a).

evacuated. Before 0 min, RH was set to  $\sim 5\%$  on the sample surface by introducing water vapor (0.5 Torr). This resulted in an increase in both  $\Delta E_{\text{GeO}_2}$  and  $\Delta E_{\text{SiO}_2}$  compared with those in the initial vacuum, which is the reason for the positive values of  $\Delta E_{\text{change}}$  at 0 min. The graph shows  $\Delta E_{\text{change}}$  after evacuation by a turbomolecular pump starting at 0 min. For the SiO<sub>2</sub>/Si samples,  $\Delta E_{\text{SiO}_2}$  monotonically decreases after 0 min. After 100 min, it becomes less than 0.1 eV and approaches 0 eV. For the GeO<sub>2</sub>/Ge samples,  $\Delta E_{\text{GeO}_2}$  decreases after 0 min, similarly to that of the SiO<sub>2</sub>/Si sample. However, it almost saturates at 0.3–0.4 eV after 200 min. This is probably due to water species remaining in the permeable GeO<sub>2</sub> films, as detected in our previous study.<sup>17</sup> This means that, in contrast to a SiO<sub>2</sub> surface, the exposure of a GeO<sub>2</sub> surface to water vapor appears to increase  $\Delta E_{\text{GeO}_2}$  even if Ge 3d spectra are subsequently obtained in a vacuum of pressure lower than  $1 \times 10^{-6}$  Torr. Mild annealing at 300 °C is effective for returning  $\Delta E_{\text{GeO}_2}$  and  $\Delta E_{\text{SiO}_2}$  to close to their initial values obtained in UHV, as indicated by dashed lines in Fig. 5. These results in Fig. 5 are in agreement with those in Fig. 2.

Figures 2–5 imply that the formation of thin water films causes increases in both  $\Delta E_{\text{GeO}_2}$  and  $\Delta E_{\text{SiO}_2}$ . One possible reason is a change in the chemical bonds of the oxide

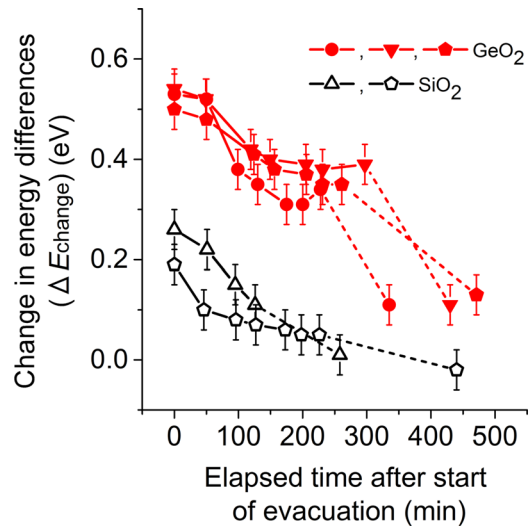


FIG. 5. Recovery properties of  $\Delta E_{\text{GeO}_2}$  and  $\Delta E_{\text{SiO}_2}$  as a function of elapsed time after the start of the evacuation of water vapor in the chamber. Dashed lines indicate how  $\Delta E_{\text{change}}$  decreases upon annealing the samples at 300 °C for 10 min. Data plotted as pentagonal symbols were obtained from Ge 3d and Si 2p spectra with incident photon energies of 250 and 320 eV, respectively. These values ensure that photoelectrons had a similar kinetic energy of  $\sim 220$  eV, whereas all other data were obtained using photoelectrons with a kinetic energy of  $\sim 320$  eV.

network (i.e., the initial state change), but this can be ruled out because of the following results. Figure 6 shows the energy difference between the oxide (Ge<sup>4+</sup>) and substrate Ge 3d<sub>5/2</sub> peaks ( $\Delta E_{\text{GeO}_2}$ ) [plots in (a)], and that between the oxide in O 1s and Ge<sup>4+</sup> in Ge 3d<sub>5/2</sub> peaks ( $\Delta E_{\text{O-Ge}}$ ) [plots in (b)] as a function of RH. Ge 3d and O 1s spectra for the plots in Fig. 6 were collected at an incident photon energy of 855 eV. As shown in the insets, Ge 3d and O 1s spectra were peak-fitted, the procedures of which are the same as those in the cases of Figs. 2 and 1, respectively. In contrast to the rapid increase in  $\Delta E_{\text{GeO}_2}$  at higher RH in Fig. 6(a),  $\Delta E_{\text{O-Ge}}$  is nearly constant, as shown in Fig. 6(b). We conducted the same experiment as that in the case of Fig. 6 with Si 2p and O 1s spectra, and a trend similar to that in Fig. 6 was confirmed. These results indicate that the larger  $\Delta E_{\text{GeO}_2}$  and  $\Delta E_{\text{SiO}_2}$  at higher RH do not represent a change in the initial bonding states.

A straightforward explanation of the increases in  $\Delta E_{\text{GeO}_2}$  and  $\Delta E_{\text{SiO}_2}$  with thin water films is positive charging of the oxide films. We discuss its origin from the viewpoint of X-ray irradiation. Figure 7 shows the result of the time-lapse measurement of  $\Delta E_{\text{SiO}_2}$  upon the X-ray irradiation of SiO<sub>2</sub>/Si samples. The data in Figs. 7(a) and 7(b) were obtained in UHV and at 2.3% RH, respectively. Fig. 8 shows the expected band diagrams of the SiO<sub>2</sub>/Si structures. In both graphs in Fig. 7, 0 min indicates the start of X-ray irradiation on an area of the surface that had not been exposed to X-rays. In Fig. 7(a), the initial  $\Delta E_{\text{SiO}_2}$  is 3.95 eV. The schematic band diagram to exhibit this initial  $\Delta E_{\text{SiO}_2}$  is assumed as Fig. 8(a).  $\Delta E_{\text{SiO}_2}$  in Fig. 7(a) gradually increases to approximately 4.1 eV at 200 s, after which remains almost constant until 700 s. This increase in  $\Delta E_{\text{SiO}_2}$  is due to the insulating SiO<sub>2</sub> film being positively charged by the emission of photoelectrons by X-ray irradiation. In other words, the

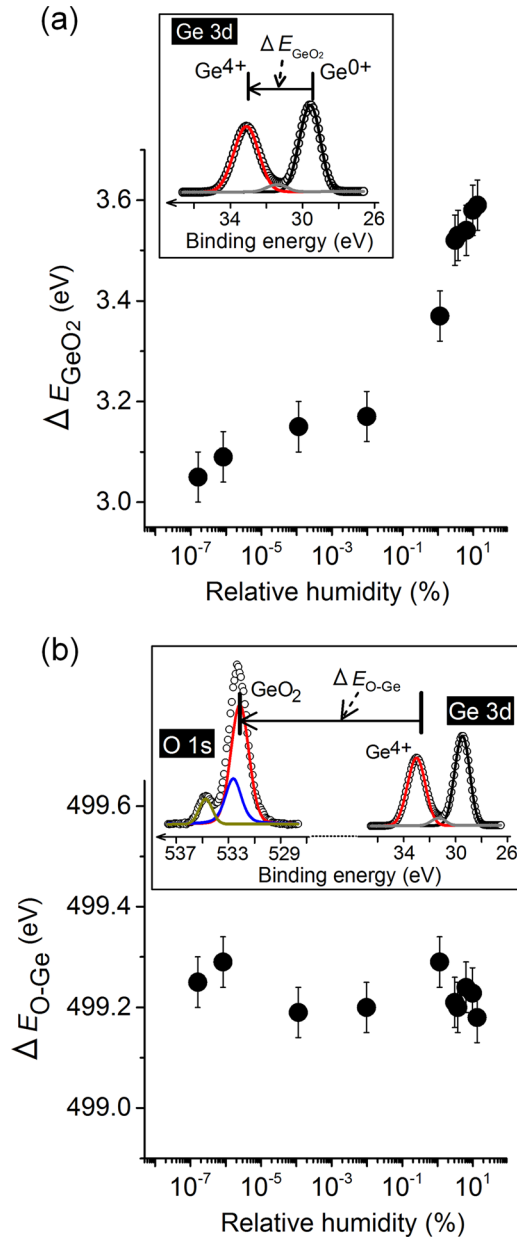


FIG. 6. (a) Energy differences as a function of RH (a) between the oxide ( $\text{Ge}^{4+}$ ) and substrate Ge  $3d_{5/2}$  peaks in Ge 3d spectra ( $\Delta E_{\text{GeO}_2}$ ) and (b) between the oxide in O 1s and oxide ( $\text{Ge}^{4+}$ ) Ge  $3d_{5/2}$  peaks ( $\Delta E_{\text{O-Ge}}$ ). In the O 1s spectrum in the inset in (b), red, blue and, other curves represent  $\text{GeO}_2$ , adsorbed  $\text{H}_2\text{O}$  including hydroxyls and gas-phase  $\text{H}_2\text{O}$ , respectively. Both O 1s and Ge 3d spectra were taken at the same photon energy of 855 eV. The  $\text{GeO}_2$  thickness was 1.85 nm. Each data plot in (a) and (b) has an error of  $\pm 0.05$  eV.

loss of electrons in the  $\text{SiO}_2$  layer is not completely compensated only by tunneling electrons from the Si substrate. This creates a downward potential drop of  $\Delta V_{\text{ox}}$  across the oxide layer, whose band diagram is schematically shown in Fig. 8(b).<sup>40</sup> This  $\Delta V_{\text{ox}}$  is the origin of the increase in  $\Delta E_{\text{SiO}_2}$  by prolonged X-ray irradiation of the structure in Fig. 7(a). In Fig. 7(b),  $\Delta E_{\text{SiO}_2}$  increases rapidly by approximately 0.15 eV up to 200 s and then saturates. The net change in  $\Delta E_{\text{SiO}_2}$  upon the prolonged irradiation of X-rays shown in Fig. 7(b) is 0.05–0.07 eV larger than that in Fig. 7(a). On the basis of the result in Fig. 3, the  $\text{SiO}_2$  surface in Fig. 7(b) was probably covered by a one-monolayer water film. Because of the

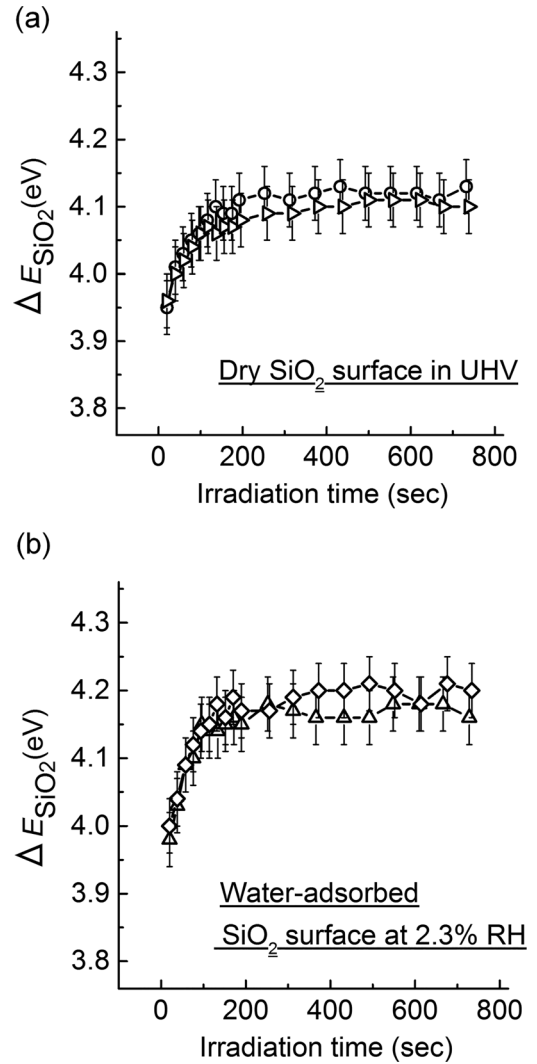


FIG. 7.  $\Delta E_{\text{SiO}_2}$  as a function of elapsed time after the start of X-ray irradiation. (a) and (b) show the results obtained in UHV and in water vapor, respectively. The plots with different symbols were obtained on different areas of the surface of a  $\text{SiO}_2/\text{Si}$  sample with an oxide thickness of 2.36 nm that had not been exposed to X-rays. Each plot was obtained from a single Si 2p spectrum, rather than an averaged spectrum obtained from multiple raw spectra. Although this reduced the signal-to-noise ratio of the spectrum, it enabled us to rapidly obtain a spectrum in 18–20 s.

interaction of this thin water film, or adsorbed water species, with the X-ray beam, positive charging is enhanced compared with that for a dry  $\text{SiO}_2$  surface (Fig. 7(a)). The expected band diagram in the case of both X-ray irradiation and water vapor is drawn in Fig. 8(c). The enhanced  $\Delta V_{\text{ox}}$  explains why  $\Delta E_{\text{SiO}_2}$  increases greatly on water-adsorbed  $\text{SiO}_2$  under X-ray irradiation as shown in Fig. 7. Next, we used  $\text{GeO}_2/\text{Ge}$  samples to conduct similar experiments to those in Fig. 7, the results of which are shown in Fig. 9. We assume Fig. 10(a) to be the initial band diagram for a dry  $\text{GeO}_2$  surface on Ge after preannealing. As shown in Fig. 9(a),  $\Delta E_{\text{GeO}_2}$  increases again by approximately 0.1 eV in 300 s after the start of X-ray irradiation of a dry  $\text{GeO}_2$  surface. This increase is due to the positive charging of the  $\text{GeO}_2$  surface by X-ray irradiation or a downward potential drop of  $\Delta V_{\text{ox}}$  across the oxide layer, whose band diagram is schematically shown in Fig. 10(b). In Fig. 9(b),  $\Delta E_{\text{GeO}_2}$

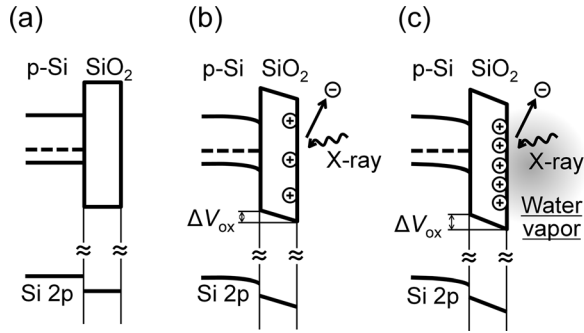


FIG. 8. Band diagrams for the SiO<sub>2</sub>/Si structure. (a) and (b) Diagrams in UHV without and with X-ray irradiation, respectively. (c) With X-ray irradiation in water vapor.

increases monotonically during X-ray irradiation, and its increase reaches 0.15–0.2 eV after 700 s. This X-ray-induced positive charging appears to be more significant by 0.05–0.10 eV on a water-adsorbed GeO<sub>2</sub> surface than on a

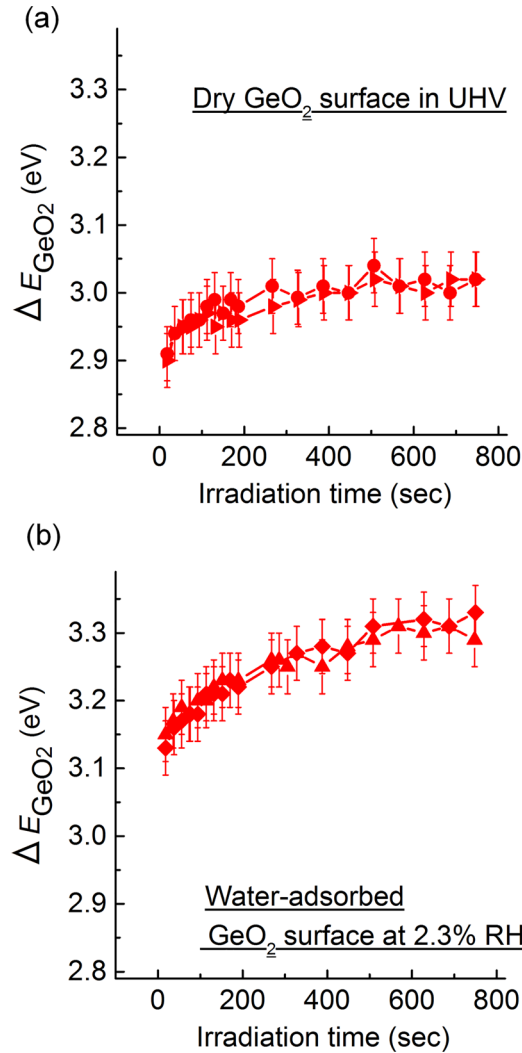


FIG. 9.  $\Delta E_{\text{GeO}_2}$  as a function of elapsed time after the start of X-ray irradiation. The oxide thickness of the GeO<sub>2</sub>/Ge sample was estimated to be 1.39 nm. The plots with different symbols were obtained on different areas of the surface that had not been exposed to X-rays. As mentioned in Fig. 7, each plot was obtained from a single Ge 3d spectrum to rapidly obtain a spectrum in 18–20 s.

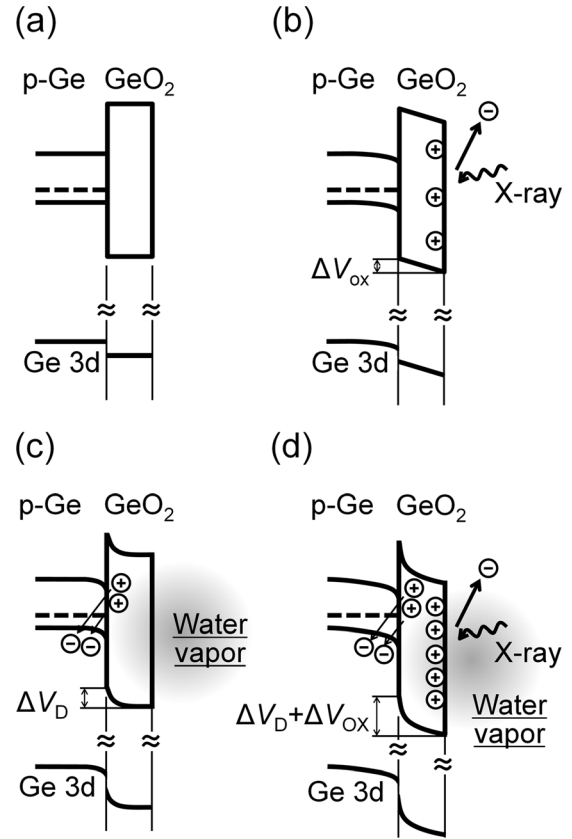


FIG. 10. Band diagrams for the GeO<sub>2</sub>/Ge structure. (a) and (b) Diagrams in UHV without and with X-ray irradiation, respectively. (c) and (d) Diagrams on water-adsorbed GeO<sub>2</sub>/Ge without and with X-ray irradiation, respectively.

dry GeO<sub>2</sub> surface; this difference is similar to that for the SiO<sub>2</sub>/Si samples shown in Fig. 7. What is striking is that the initial  $\Delta E_{\text{GeO}_2}$  appears to be about 0.2 eV larger in Fig. 9(b) than in Fig. 9(a). This is contrary to the result for the SiO<sub>2</sub>/Si samples in Fig. 7, in which the initial  $\Delta E_{\text{SiO}_2}$  does not change significantly in the presence of a thin water film. This is likely to be unrelated to the X-ray irradiation, i.e., a *non*-X-ray effect, where the GeO<sub>2</sub> film is positively charged spontaneously by the adsorption of water molecules.

To investigate the validity of this idea, we conducted another time-lapse measurement. Figure 11 shows the results, in which all the Si 2p and Ge 3d spectra were recorded with the same photon energy of 855 eV. The plots in Fig. 11 fluctuate because the photon flux of the X-rays used was lower than half of those in Figs. 7 and 9, which made it difficult to accurately conduct a peak-fitting analysis of the Si 2p or Ge 3d spectra. One important point in Fig. 11 is that the X-ray effect, i.e., the increase in the energy difference from the first plot to the last plot at approximately 800 s, appears to be less than those in Figs. 7 and 9, which is likely due to the smaller flux of X-rays in Fig. 11. We speculate from this result that the amount of positive charging of the oxide during X-ray irradiation depends on the X-ray conditions such as intensity and photon energy. Even more importantly, in the case of GeO<sub>2</sub>/Ge, there is a marked increase in  $\Delta E_{\text{GeO}_2}$  of approximately 0.2 eV between the first plots in Figs. 11(c) and 11(d). On the other hand, this *non*-X-ray effect is absent in the SiO<sub>2</sub>/Si system in Figs. 11(a) and 11(b).



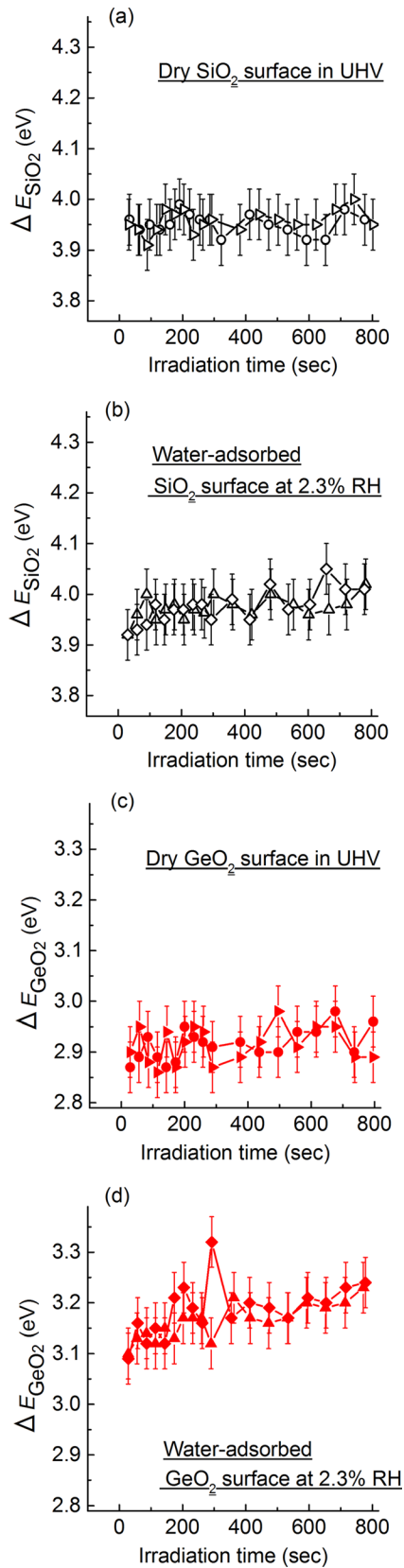


FIG. 11. (a) and (b)  $\Delta E_{\text{SiO}_2}$  as a function of elapsed time after the start of X-ray irradiation of a 1.73-nm-thick SiO<sub>2</sub> film on Si. (c) and (d)  $\Delta E_{\text{GeO}_2}$  as a function of elapsed time after the start of X-ray irradiation of a 1.51-nm-thick-GeO<sub>2</sub> film on Ge. The plots with different symbols were obtained on different areas of the SiO<sub>2</sub> or GeO<sub>2</sub> surface that had not been exposed to X-rays. All the raw Si 2p and Ge 3d spectra in (a)–(d) were obtained with the same incident photon energy (855 eV). It took 28–30 s to obtain each spectrum. Each data plot in (a)–(d) has an error of  $\pm 0.05$  eV.

The results in Fig. 11 support our interpretation of the results in Fig. 9(b), in which the formation of a thin water film is considered to cause positive charging of a GeO<sub>2</sub> film that is unrelated to the X-ray irradiation. It took about 20 and 30 s to obtain the first plots in Figs. 9(b) and 11(d), respectively, after the start of X-ray irradiation. If some positive charges in GeO<sub>2</sub> films were built up by X-rays in a much shorter time scale, we would not be able to detect them as an X-ray-induced effect. However, the initial difference in  $\Delta E_{\text{GeO}_2}$  between the first plots in Figs. 11(c) and 11(d) is similar to that in Figs. 9(a) and 9(b) in spite of the reduced flux of the X-rays, as mentioned in the previous paragraph. For this reason, although there is room for further investigation, we discuss the origin of the higher  $\Delta E_{\text{GeO}_2}$  on the water-adsorbed GeO<sub>2</sub> film from the viewpoint of a *non-X-ray* effect.

Considering the permeability of GeO<sub>2</sub>, a likely explanation is that electrons are transferred from the water-related species in GeO<sub>2</sub> to the Ge bulk upon exposure to water vapor, which causes positive charging of the films. A pioneering work in the 1970s showed that water molecules impacting on the surface of a GeO<sub>2</sub> film are instantaneously adsorbed and slowly diffuse deep into the film. This diffusion is paralleled by the fixation of H<sub>2</sub>O on chemisorption sites in the film, accompanied by the ionization of H<sub>2</sub>O molecules, causing them to emit electrons in the Ge bulk.<sup>42</sup> More recently, the generation of positive charges in GeO<sub>2</sub> films after exposure to air has been confirmed by a negative shift of  $V_{\text{FB}}$  in the capacitance-voltage ( $C$ - $V$ ) characteristics of metal/GeO<sub>2</sub>/Ge diodes.<sup>12–14</sup> Because the  $C$ - $V$  characteristics can be used to sense electrical properties, especially at an oxide/semiconductor interface, these results indicate that water molecules in air infiltrate the GeO<sub>2</sub> film, reaching the GeO<sub>2</sub>/Ge interface, where they create positive charges. These reports agree with our data in Figs. 9(b) and 11(d), which show the spontaneous positive charging of the GeO<sub>2</sub> film by water adsorption.

In Fig. 4, in contrast to  $\Delta E_{\text{SiO}_2}$ ,  $\Delta E_{\text{GeO}_2}$  begins to increase rapidly at a very low humidity of  $10^{-4}\%$ . As we reported previously, the increase in  $\Delta E_{\text{GeO}_2}$  saturates above about 10% RH.<sup>17</sup> This means that this rapid increase in  $\Delta E_{\text{GeO}_2}$ , or the generation of positive charges discussed above, is related to a structural change in the GeO<sub>2</sub> film that occurs in this low-RH range. A plausible explanation for this change is the partial hydroxylation of the film. As mentioned in the discussion of Fig. 3, we speculate that hydroxylation of the GeO<sub>2</sub> film occurred in the RH range between  $\sim 10^{-4}$  and 1%. Then, what is the microscopic mechanism that creates positive charges in a partially hydroxylated GeO<sub>2</sub> film up to 1% RH? We previously reported the dependence of the suboxide structures of GeO<sub>2</sub>/Ge samples on RH.<sup>17</sup> Although the peak areas of suboxides (Ge<sup>1+</sup>, Ge<sup>2+</sup>, Ge<sup>3+</sup>) in Ge 3d spectra changed only slightly with the RH, we found that the peak area of Ge<sup>2+</sup> tended to decrease gradually at an elevated RH up to  $\sim 1\%$ , whereas that of Ge<sup>3+</sup> increased monotonically. One example is shown in Fig. 2, in which the peak area of Ge<sup>2+</sup> after preannealing in Fig. 2(b) is larger than that after air exposure with water vapor in Fig. 2(a). It was deduced that the initial abrupt GeO<sub>2</sub>/Ge interface that existed after annealing in UHV collapsed upon hydroxylation at a

low RH of up to  $\sim 1\%$  RH. This agrees with the result of a dynamic SIMS analysis of an air-exposed  $\text{GeO}_2/\text{Ge}$  sample, in which a certain amount of hydrogen was detected near the  $\text{GeO}_2/\text{Ge}$  interface.<sup>15</sup> It is likely that infiltrated water molecules promote hydroxylation to generate hole-trap states in the  $\text{GeO}_2$  films, especially near the  $\text{GeO}_2/\text{Ge}$  interface or in the suboxide layer. These traps above the Ge Fermi level in the suboxide layer are positively charged by the electrons emitted to the Ge bulk, as suggested by Oniki and Ueno.<sup>13</sup> These positively charged states, or immobile cations, may be the origin of the *non*-X-ray-induced positive charging suggested by our XPS results in Figs. 9 and 11. Figures 10(c) and 10(d) depict the band diagrams of the water-adsorbed  $\text{GeO}_2/\text{Ge}$  system without and with X-ray irradiation, respectively. Unlike  $\text{SiO}_2/\text{Si}$ , a downward potential drop, or  $\Delta V_D$  in Fig. 10(c), occurs spontaneously in a water-adsorbed  $\text{GeO}_2$  film near the  $\text{GeO}_2/\text{Ge}$  interface. Because X-ray irradiation induces an additional potential drop ( $\Delta V_{\text{ox}}$ ), the total change in the potential ( $\Delta V_D + \Delta V_{\text{ox}}$ ) becomes rather large upon X-ray irradiation in water vapor, as shown in Fig. 10(d). This large potential drop across the  $\text{GeO}_2$  layer ( $\Delta V_D + \Delta V_{\text{ox}}$ ) explains the significant increase in  $\Delta E_{\text{GeO}_2}$  on a water-adsorbed  $\text{GeO}_2/\text{Ge}$  structure under X-ray irradiation in Figs. 9 and 11.

It is worth noting that the quality of a  $\text{GeO}_2$  film can affect the amount of spontaneous positive charging of the  $\text{GeO}_2$  film by water adsorption. It is widely accepted that the reaction at the  $\text{GeO}_2/\text{Ge}$  interface induced by heat treatment can cause GeO volatilization as follows:<sup>3</sup>



This GeO volatilization is known to occur even during a thermal oxidation process.<sup>43</sup> As discussed above with Fig. 10(c), infiltrated water molecules cause hydroxylation to generate hole-trap states in the suboxide layer of  $\text{GeO}_2$  films. Thus, the hole-trap density is likely to depend on the thickness of the suboxide layer, which is determined by the GeO volatilization during the oxide growth. It is also imagined that the amount of infiltrated water molecules in the  $\text{GeO}_2$  film itself is influenced by the suboxide layer thickness. Low-temperature oxidation, such as at  $400^\circ\text{C}$ , is reported to be effective for reducing the suboxide layer thickness due to the suppression of GeO volatilization.<sup>14</sup> In our experiments, the oxidation temperature used to form  $\text{GeO}_2$  films was set to  $550^\circ\text{C}$ . If a  $\text{GeO}_2$  film is formed at a lower temperature such as  $400^\circ\text{C}$ , the suboxide layer will be thinner, leading to a lower hole-trap density. In such a case, the increase of  $\Delta E_{\text{GeO}_2}$  due to the adsorption of water molecules, which was about 0.2 eV in Figs. 11(c) and 11(d), may be suppressed.

In Figs. 9(a) and 11(c), the initial  $\Delta E_{\text{Ge}}$  on the newly annealed  $\text{GeO}_2$  film is plotted as  $\sim 2.9$  eV. This value is almost equal to the result for a thin Ge oxide film obtained by Matsui *et al.*<sup>29</sup> but much smaller than other values obtained by XPS such as 3.4 eV (Ref. 44) and 3.46 eV.<sup>45</sup> Then, what is the true chemical shift of a pure  $\text{GeO}_2$  layer? One may think that the smaller value of  $\Delta E_{\text{GeO}_2}$  is more accurate because water adsorption and X-ray-induced positive charging both increase  $\Delta E_{\text{GeO}_2}$ . On the other hand, in the

case of  $\text{SiO}_2/\text{Si}$ , many groups have reported the factors determining  $\Delta E_{\text{SiO}_2}$ . In addition to charging and the change in chemical bonds, a final-state effect<sup>37</sup> is considered to be a key factor. This effect refers to a mechanism that stabilizes (or destabilizes) the core-hole state that is formed upon the ejection of a photoelectron from an emitting atom.<sup>39</sup> Namely, in a  $\text{SiO}_2/\text{Si}$  system, electrons ejected from the Si atoms in  $\text{SiO}_2$  have a reduced binding energy due to the Coulomb interaction with the core holes because they are also subjected to the repulsion (screening) of their image charges in the Si bulk.<sup>41</sup> This effect is more significant in thinner  $\text{SiO}_2$  films, and researchers have argued that the larger  $\Delta E_{\text{SiO}_2}$  for a thicker  $\text{SiO}_2$  layer of up to 2–3 nm thickness is mainly caused by this final-state effect.<sup>39–41</sup> Our small  $\Delta E_{\text{GeO}_2}$  of  $\sim 2.9$  eV in Figs. 9(a) and 11(c) may have been affected by the final-state effect because it was obtained with a  $\text{GeO}_2$  film of thickness less than 2 nm. As demonstrated by another group<sup>40</sup> for the case of a  $\text{SiO}_2/\text{Si}$  system, the XPS spectra obtained on metal-coated  $\text{GeO}_2/\text{Ge}$  structures are expected to reveal more details on the actual chemical shift of the pure  $\text{GeO}_2$  film.

The point of this study is that  $\Delta E_{\text{GeO}_2}$  increases significantly when a  $\text{GeO}_2$  film on a Ge bulk is partially hydroxylated. It is well known for  $\text{SiO}_2/\text{Si}$  that  $\Delta E_{\text{SiO}_2}$  depends on the oxide thicknesses, and it is plausible that beam conditions such as the X-ray intensity and photon energy are also factors affecting  $\Delta E_{\text{SiO}_2}$ . In addition to these parameters, water adsorption greatly affects  $\Delta E_{\text{GeO}_2}$ . The amount of absorbed water molecules, or the extent of hydroxylation of the  $\text{GeO}_2$  layer, depends on the sample preparation and the transfer method. For this reason, even in conventional XPS measurements in UHV, values of  $\Delta E_{\text{GeO}_2}$  can be much more scattered than those of  $\Delta E_{\text{SiO}_2}$  among different experiments and research groups. But if we carefully analyze the measured  $\Delta E_{\text{GeO}_2}$ , it can be used to evaluate the quality of a thin Ge oxide.

#### IV. CONCLUSION

We conducted AP-XPS measurements of thin thermal  $\text{GeO}_2/\text{Ge}$  samples to investigate the relationship between the peak shift of an oxide ( $\text{Ge}^{4+}$ ) from the bulk and the water layer thickness. This was achieved by using an AP-XPS setup to collect photoelectrons in water vapor up to a pressure of Torr order together with control of the sample temperature or RH on an oxide surface. We compared the results with those for thermally oxidized  $\text{SiO}_2$  films on Si substrates. For similar beam intensities, we revealed that both  $\Delta E_{\text{GeO}_2}$  and  $\Delta E_{\text{SiO}_2}$  increase at an elevated RH of up to  $\sim 5\%$  and that this trend is much clearer for  $\Delta E_{\text{GeO}_2}$ . More specifically, the increase of  $\Delta E_{\text{change}}$  for  $\text{GeO}_2/\text{Ge}$  is moderate up to  $\sim 10^{-4}\%$  RH, which is similar to that for  $\text{SiO}_2/\text{Si}$ . After that, in contrast to  $\Delta E_{\text{SiO}_2}$ ,  $\Delta E_{\text{GeO}_2}$  rapidly increases. Because the rapid growth of a water layer also starts above this critical RH ( $10^{-4}\%$ ), we expect that the increase in  $\Delta E_{\text{GeO}_2}$  is caused by adsorbed water, rather than other species such as carbon-based contaminants. We find that  $\Delta E_{\text{GeO}_2}$  remains larger than that of the initial annealed  $\text{GeO}_2/\text{Ge}$  sample once it is exposed to water vapor at  $\sim 5\%$  RH, even if this vapor is

evacuated. This is more apparent for GeO<sub>2</sub>/Ge than for SiO<sub>2</sub>/Si, which indicates that  $\Delta E_{\text{GeO}_2}$  depends on the amount of infiltrated water molecules in a GeO<sub>2</sub> layer. We also performed the time-lapse measurement of  $\Delta E_{\text{GeO}_2}$  and  $\Delta E_{\text{SiO}_2}$  after the start of X-ray irradiation on water-adsorbed oxide surfaces. It turned out that both SiO<sub>2</sub> and GeO<sub>2</sub> films are positively charged by X-ray irradiation and that this X-ray-induced positive charging is greater on water-adsorbed oxide surfaces than that on dry oxide surfaces. What was striking in this time-lapse measurement was that the initial  $\Delta E_{\text{GeO}_2}$  for water-adsorbed GeO<sub>2</sub>/Ge was  $\sim 0.2$  eV higher than that of newly annealed GeO<sub>2</sub>/Ge whereas no such difference was observed for SiO<sub>2</sub>/Si. There are several possible explanations to account for this energy difference. One is beam-induced charging, in which the positive charging of a water-adsorbed GeO<sub>2</sub> film occurs most rapidly in the first 10–20 s after the start of irradiation. Another possibility is the intrinsic positive charging of a GeO<sub>2</sub> film upon water adsorption, which is caused by electron transfer from water species in the suboxide layer of a partially hydroxylated GeO<sub>2</sub> film to the Ge bulk. This intrinsic charging may be relevant to the negative shift of  $V_{\text{FB}}$  in MOS diodes with an air-exposed GeO<sub>2</sub> film. We obtained  $\Delta E_{\text{GeO}_2}$  of  $\sim 2.9$  eV on a 1.4-nm-thick GeO<sub>2</sub> film with neither adsorbed water molecules nor prolonged X-ray irradiation, which is smaller than the values in most reports. It follows from this study that special attention should be paid to the oxide peak in XPS spectra obtained from permeable oxide films.

## ACKNOWLEDGMENTS

The authors wish to thank Dr. Hendrik Bluhm, Dr. Stephanus Axnanda, Sana Rani, Yusuke Saito, Yoshie Kawai, and Yuya Minoura for the operation of AP-XPS and valuable advice. This work was supported by the Japan Society for the Promotion of Science (JSPS) KAKENHI Grant Nos. JP24686020, JP26630026 and JP16K14133. This work was also supported in part by a grant from the Murata Science Foundation and the Mikiya Science and Technology Foundation. The Advanced Light Source is supported by the Director, Office of Science, Office of Basic Energy Sciences, of the U.S. Department of Energy under Contract No. DE-AC02-05CH11231.

<sup>1</sup>J. Robertson, *Rep. Prog. Phys.* **69**, 327 (2006).

<sup>2</sup>H. Shang, M. M. Frank, E. P. Gusev, J. O. Chu, S. W. Bedell, K. W. Guarini, and M. Jeong, *IBM J. Res. Dev.* **50**, 377 (2006).

<sup>3</sup>K. Kita, S. Suzuki, H. Nomura, T. Takahashi, T. Nishimura, and A. Toriumi, *Jpn. J. Appl. Phys., Part 1* **47**, 2349 (2008).

<sup>4</sup>K. Kita, S. Suzuki, H. Nomura, T. Takahashi, T. Nishimura, and A. Toriumi, *ECS Trans.* **11**, 461 (2007).

<sup>5</sup>K. Prabhakaran and T. Ogino, *Surf. Sci.* **325**, 263 (1995).

<sup>6</sup>H. Matsubara, T. Sasada, M. Takenaka, and S. Takagi, *Appl. Phys. Lett.* **93**, 032104 (2008).

<sup>7</sup>K. Kutsuki, G. Okamoto, T. Hosoi, T. Shimura, and H. Watanabe, *Appl. Phys. Lett.* **95**, 022102 (2009).

<sup>8</sup>F. Bellenger, M. Houssa, A. Delabie, V. V. Afanas'ev, T. Conard, M. Caymax, M. Meuris, K. De Meyer, and M. M. Heyns, *J. Electrochem. Soc.* **155**, G33 (2008).

<sup>9</sup>A. Delabie, F. Bellenger, M. Houssa, T. Conard, S. Van Elshocht, M. Caymax, M. Heyns, and M. Meuris, *Appl. Phys. Lett.* **91**, 082904 (2007).

<sup>10</sup>C. M. Lu, C. H. Lee, W. F. Zhang, T. Nishimura, K. Nagashio, and A. Toriumi, *Appl. Phys. Lett.* **104**, 092909 (2014).

<sup>11</sup>C. Lu, C. H. Lee, W. Zhang, T. Nishimura, K. Nagashio, and A. Toriumi, *J. Appl. Phys.* **116**, 174103 (2014).

<sup>12</sup>T. Hosoi, K. Kutsuki, G. Okamoto, M. Saito, T. Shimura, and H. Watanabe, *Appl. Phys. Lett.* **94**, 202112 (2009).

<sup>13</sup>Y. Oniki and T. Ueno, *Appl. Phys. Express* **4**, 081101 (2011).

<sup>14</sup>Y. Oniki and T. Ueno, *Jpn. J. Appl. Phys., Part 1* **51**, 04DA01 (2012).

<sup>15</sup>S. Ogawa, T. Suda, T. Yamamoto, K. Kutsuki, I. Hideshima, T. Hosoi, T. Shimura, and H. Watanabe, *Appl. Phys. Lett.* **99**, 142101 (2011).

<sup>16</sup>W. F. Zhang, T. Nishimura, K. Nagashio, K. Kita, and A. Toriumi, *Appl. Phys. Lett.* **102**, 102106 (2013).

<sup>17</sup>A. Mura, I. Hideshima, Z. Liu, T. Hosoi, H. Watanabe, and K. Arima, *J. Phys. Chem. C* **117**, 165 (2013).

<sup>18</sup>S. Morita, A. Shinozaki, Y. Morita, K. Nishimura, T. Okazaki, S. Urabe, and M. Morita, *Jpn. J. Appl. Phys., Part 1* **43**, 7857 (2004).

<sup>19</sup>M. E. Grass, P. G. Karlsson, F. Aksoy, M. Lundqvist, B. Wannberg, B. S. Mun, Z. Hussain, and Z. Liu, *Rev. Sci. Instrum.* **81**, 053106 (2010).

<sup>20</sup>D. F. Ogletree, H. Bluhm, G. Lebedev, C. S. Fadley, Z. Hussain, and M. Salmeron, *Rev. Sci. Instrum.* **73**, 3872 (2002).

<sup>21</sup>M. Salmeron and R. Schlögl, *Surf. Sci. Rep.* **63**, 169 (2008).

<sup>22</sup>NIST X-ray Photoelectron Spectroscopy Database; National Institute of Standards and Technology: Gaithersburg, MD.

<sup>23</sup>C. J. Powell, *J. Electron Spectrosc. Relat. Phenom.* **185**, 1 (2012).

<sup>24</sup>Note that the bulk peak of Ge was fixed at 29.7 eV in our previous paper,<sup>17</sup> which was reported as the value for Ge 3d.<sup>22</sup> Because we found 29.36 eV to be the binding energy of a more specific Ge 3d<sub>5/2</sub> core line signal for the Ge bulk,<sup>23</sup> we used it as the energy reference for the measured Ge 3d spectra.

<sup>25</sup>NIST Electron Inelastic-Mean-Free-Path Database; National Institute of Standards and Technology: Gaithersburg, MD.

<sup>26</sup>F. J. Himpsel, F. R. McFeely, A. Taleb Ibrahim, J. A. Yarnoff, and G. Hollinger, *Phys. Rev. B* **38**, 6084 (1988).

<sup>27</sup>K. Arima, P. Jiang, X. Y. Deng, H. Bluhm, and M. Salmeron, *J. Phys. Chem. C* **114**, 14900 (2010).

<sup>28</sup>A. Verdager, C. Weis, G. Oncins, G. Ketteler, H. Bluhm, and M. Salmeron, *Langmuir* **23**, 9699 (2007).

<sup>29</sup>M. Matsui, H. Murakami, T. Fujioka, A. Ohta, S. Higashi, and S. Miyazaki, *Microelectron. Eng.* **88**, 1549 (2011).

<sup>30</sup>D. B. Asay and S. H. Kim, *J. Phys. Chem. B* **109**, 16760 (2005).

<sup>31</sup>A. L. Sumner, E. J. Menke, Y. Dubowski, J. T. Newberg, R. M. Penner, J. C. Hemminger, L. M. Wingen, T. Brauers, and B. J. Finlayson-Pitts, *Phys. Chem. Chem. Phys.* **6**, 604 (2004).

<sup>32</sup>G. Ketteler, S. Yamamoto, H. Bluhm, K. Andersson, D. E. Starr, D. F. Ogletree, H. Ogasawara, A. Nilsson, and M. Salmeron, *J. Phys. Chem. C* **111**, 8278 (2007).

<sup>33</sup>X. Deng, T. Herranz, C. Weis, H. Bluhm, and M. Salmeron, *J. Phys. Chem. C* **112**, 9668 (2008).

<sup>34</sup>S. Yamamoto, T. Kendelewicz, J. T. Newberg, G. Ketteler, D. E. Starr, E. R. Mysak, K. J. Andersson, H. Ogasawara, H. Bluhm, M. Salmeron, G. E. Brown, and A. Nilsson, *J. Phys. Chem. C* **114**, 2256 (2010).

<sup>35</sup>J. T. Newberg, D. E. Starr, S. Yamamoto, S. Kaya, T. Kendelewicz, E. R. Mysak, S. Porsgaard, M. B. Salmeron, G. E. Brown, A. Nilsson, and H. Bluhm, *J. Phys. Chem. C* **115**, 12864 (2011).

<sup>36</sup>S. Yamamoto, K. Andersson, H. Bluhm, G. Ketteler, D. E. Starr, T. Schiros, H. Ogasawara, L. G. M. Pettersson, M. Salmeron, and A. Nilsson, *J. Phys. Chem. C* **111**, 7848 (2007).

<sup>37</sup>G. Hollinger, *Appl. Surf. Sci.* **8**, 318 (1981).

<sup>38</sup>S. Iwata and A. Ishizaka, *J. Appl. Phys.* **79**, 6653 (1996).

<sup>39</sup>K. Z. Zhang, J. N. Greeley, M. M. B. Holl, and F. R. McFeely, *J. Appl. Phys.* **82**, 2298 (1997).

<sup>40</sup>H. Kobayashi, T. Kubota, H. Kawa, Y. Nakato, and M. Nishiyama, *Appl. Phys. Lett.* **73**, 933 (1998).

<sup>41</sup>J. W. Keister, J. E. Rowe, J. J. Kolodziej, H. Niimi, H. S. Tao, T. E. Madey, and G. Lucovsky, *J. Vac. Sci. Technol. A* **17**, 1250 (1999).

<sup>42</sup>E. K. Enikeev, A. Y. Loginov, and G. F. Golovanova, *Russ. Chem. Bull.* **24**, 2044 (1975).

<sup>43</sup>Y. Oniki, H. Koumo, Y. Iwazaki, and T. Ueno, *J. Appl. Phys.* **107**, 124113 (2010).

<sup>44</sup>D. Schmeisser, R. D. Schnell, A. Bogen, F. J. Himpsel, D. Rieger, G. Landgren, and J. F. Morar, *Surf. Sci.* **172**, 455 (1986).

<sup>45</sup>Y. Wang, Y. Z. Hu, and E. A. Irene, *J. Vac. Sci. Technol. A* **12**, 1309 (1994).